The effect of the solar eclipse on the air temperature near the ground

Karol Szałowski

Faculty of Physics and Chemistry, University of Łódź, Łódź, Poland

Abstract

This paper describes the effect of the air temperature decrease in low boundary layer during the solar eclipse, with special regard to influence on convectional events. The phenomenon progress was modelled to predict solar radiation flux changes. Then the basic model of local ground and air temperature changes was constructed. The qualitative features of air temperature-time curve during the eclipse were explained. The effect was investigated experimentally on the example of the partial eclipse observed from Szczawnica, Poland on 11th August, 1999. The results of the precise air temperature measurements were presented. The general shape of temperature curve was confirmed. The problem of convection intensity and temporal scales of convectional events was examined. It was observed that the temperature variance decreased over a factor of 2 in the maximum eclipse-centred, 50 min. long time interval what depicts reduced convection regime. In addition, the temperature spectrum for long periods obtained for this time range seem to differ significantly from one registered before and after. The convection near maximum eclipse is characterised by a dominant temporal scale of 22 min., while before and after 11-13 min. scale is most important.

*e-mail address: karol_sza@wp.pl

1. Introduction

Solar eclipses (especially the total ones) belong to the astronomical phenomena that have been known and observed since the earliest ages. Their terrestrial consequences are noticeable and important. Eclipses are connected with the rapid and short-time, impulse-like decrease of solar energy flux reaching the area of its visibility, which can be exactly predicted before the occurrence of the phenomenon. Therefore, they cause noticeable changes in the atmosphere, whose main energy source is solar radiation. The strongest effects concern the layers where solar UV radiation contributes to ionisation process (ionosphere) and the boundary layer which is in direct contact with the ground absorbing shortwave radiation. Eclipses support unique, specific conditions which give the opportunity to numerous varied meteorological research. Present research works include mainly upper atmosphere studies (in most ionospheric disturbances observations – see for example Bamford, 2000), investigations concerning the influence on global and mesoscale circulation (acoustic gravity waves creation and propagation, Boska, Sauli, 2001), observations of chemical processes in the atmosphere (ozone layer changes, see Chudzyński et al., 2001). However, the effects most important for the environment take place in the microscale and involve changes of the boundary layer parameters of physical (thermodynamic processes) and chemical nature (plants response for light level decrease which causes decrease of CO_2 flux etc.). (Fabian et al., 2001). Especially the impact on air temperature can be important, as the stability and convective processes intensity changes.

2. The theoretical model of the solar eclipse phenomenon

The site of observation is characterised by its geographic co-ordinates as well as the height above the sea level. In order to describe the progress of the eclipse phenomenon, the knowledge of functions of time determining the apparent topocentric co-ordinates of the centres of the the solar and lunar disks in the equinoctial system (corrected for refraction) and their angular radii is necessary. As the diameters and distances of the celestial bodies involved are relatively small, the spherical co-ordinates system may be replaced by cartesian one to simplify further considerations. To make the description of the eclipse more practical, some useful astrometric indexes visualising the progress of the real phenomenon are usually introduced, like: the magnitude of eclipse $f(t)$, the eclipse obscuration $g(t)$ and the squared length of the chord crossing the common points of the circumferences of the solar and lunar disk $c^2(t)$, as well as the moment of the beginning of the

eclipse (the first contact t_I), the moment of the maximum t_{max} and of the end of it (the fourth

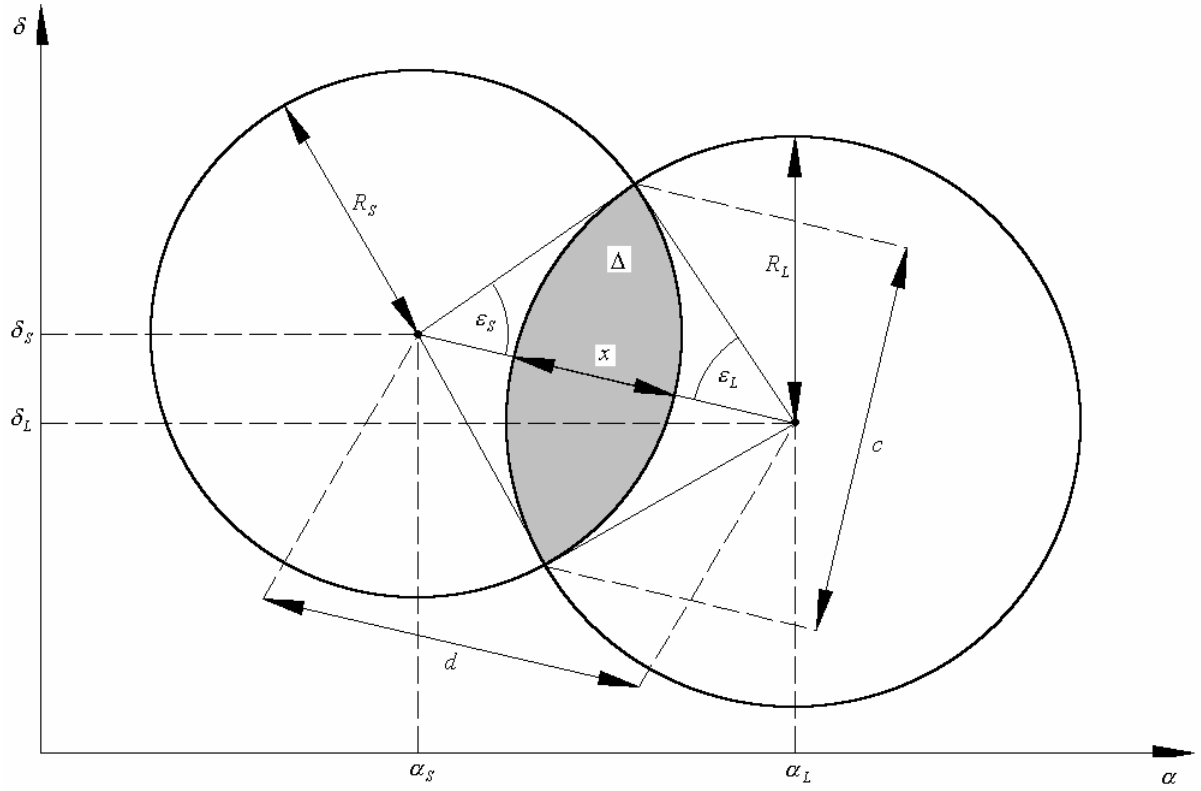contact t_{IV}) (in case of a partial eclipse).

Fig.1. Geometric model of the solar eclipse.

All quantities are considered further as time-dependent, and the values refer to the specified time

instant during the eclipse.

The most commonly used phase f is defined as a fraction of the solar disk diameter covered by

lunar disk:

$$f = \frac{x}{2R_S} \qquad (2.1)$$

x -the angular length of the part of the solar disk diameter covered by the lunar disk, R_S -angular

radius of the solar disk.

The x length is:

$$x = R_S + R_L - d \qquad (2.2)$$

R_L -the angular radius of the lunar disk, d - angular distance between the centres of solar and lunar

disk,

$$d = \sqrt{(\alpha_S - \alpha_L)^2 + (\delta_S - \delta_L)^2} \qquad (2.3)$$

The eclipse obscuration g is determined as a covered-to-total solar disk surface ratio:

$$g = \frac{\Delta}{\pi R_S{}^2} \quad (2.4)$$

On the basis of geometric considerations we get Δ as:

$$\Delta = R_S{}^2 \left(\varepsilon_S - \sin \varepsilon_S \cos \varepsilon_S \right) + R_L{}^2 \left(\varepsilon_L - \sin \varepsilon_L \cos \varepsilon_L \right) \quad (2.5),$$

where the auxiliary angles are given by:

$$\varepsilon_S = \arccos \frac{R_S{}^2 - R_L{}^2 + d^2}{2 d R_S}, \quad \varepsilon_L = \arccos \frac{R_L{}^2 - R_S{}^2 + d^2}{2 d R_L} \quad (2.6).$$

The c^2 length is very useful, especially when determining the moment of the beginning or the end of the eclipse from observations, as it can be easily measured on the images of solar disk. It is expressed by:

$$c^2 = 4 R_S{}^2 \sin^2 \varepsilon_S \quad (2.7)$$

The t_I and t_{IV} moments are determined as the times when $f(t) = 0$.

The solar eclipse of 11th August, 1999 was visible as the total one across Europe, at Middle East and in East Asia. The phenomenon was observable from Poland as a partial eclipse of large magnitude, between 81% in the Pomerania region (near Gdańsk) and 93% in some parts of Beskidy Mountains. The most advantageous conditions for observation were in south Poland (Espenak, Anderson, 1999).

Taking into consideration advantageous climate conditions (large probability of the day without cloud cover in August) and large magnitude of eclipse, Szczawnica (South Poland) was chosen for the site of observation. The geographic co-ordinates of this site (obtained in WGS 84 system from measurements at the map *Spišská Magura – Pieniny. Edícia turistických máp 1 : 50 000, 3. Vydanie, Vojenský kartografický ústav, š. p., Harmanec, 2000*) are presented below:

$$\lambda = \left(20°29'1'' \pm 4'' \right) E, \quad \varphi = \left(49°25'36'' \pm 3'' \right) N, \quad h = \left(500 \pm 10 \right) m$$

The theoretical model of the phenomenon for the site specified above was prepared on the basis of the highly accurate ephemerides for Sun and Moon provided via WWW and telnet by *JPL Horizons On-Line Ephemeris System*. The calculations covered the time range from 9[h] UT to 16[h] UT with time interval of 1 minute. The output variables were: the apparent topocentric co-ordinates in equinoctial system (corrected for refraction) and the observable angular diameter (for details see: Horizons User Manual, *http://ssd.jpl.nasa.gov/horizons_doc.html*). On the basis of the mentioned tables, the values of eclipse parameters, such as f and g were calculated using the presented model of phenomenon. The determined values of f and g are plotted below (Fig. 2):
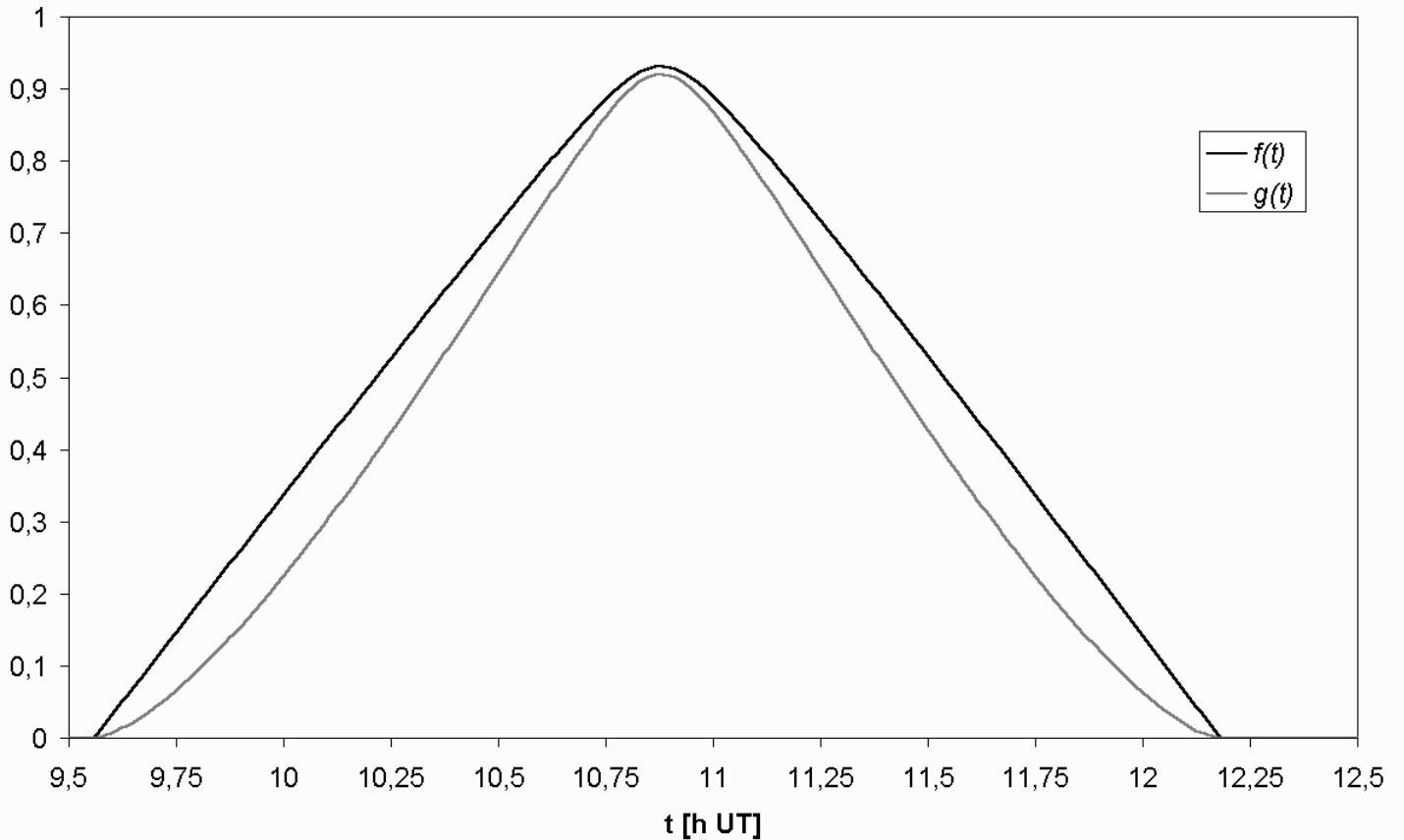
Fig.2. Astrometric parameters during the 11th August 1999 eclipse in Szczawnica.

The time moments t_I and t_{IV} were obtained from the Win-OCCULT v. 2.0.0 software (International Occultation Timing Organisation, ftp://ftp.lunar-occultations.com/pub/Windows - Occult 2.0/), as the model presented above is simplified and does not support enough accuracy to determine such moments (while being sufficient for estimating g progress for radiation changes model).

Table 1. Characteristic parameters of the eclipse in Szczawnica.

First contact t_I	Maximum of eclipse t_{max}	Fourth contact t_{IV}	Maximal magnitude f_{max}
9 h 30 m 44 s	10 h 52 m 38 s	12 h 13 m 11 s	0.932

The auxiliary observations included the recording of the phenomenon progress in real time using video camcorder with CCD of 1/3" diagonal were lead. The lens of focal length 66.3 mm and diameter 35 mm was protected with welder's filter of optical density of 12 (additional 6 and 12 filters were used if needed due to changeable cloud cover). The front part of the camera was

covered up by reflecting screen to prevent intensive heating. Its aim was to register the moments when the solar disk was covered by clouds.

3. The theoretical model of the near-ground air temperature changes during the solar eclipse

In the area covered by umbra or penumbra the change of the flux of incident solar radiation takes place. It involves decrease of the flux as well as the modifications of the spectral distribution of the incident radiation (due to spectral dependence of limb darkening, Koepke et al., 2001). The lunar shadow cone has an usual diameter of the order of magnitude of 10^3 km (Fig. 3), so it contributes to noticeable changes even in mesoscale in meteorological parameters at that area.
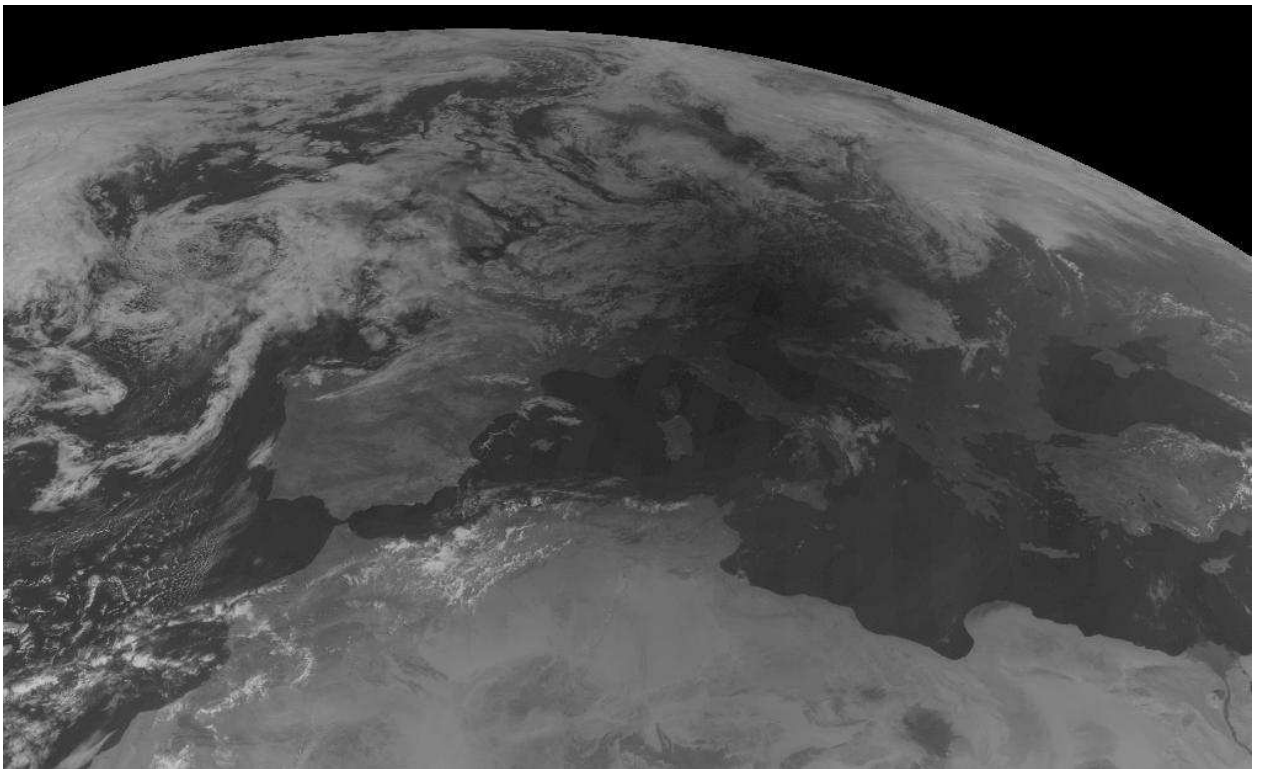

Fig.3. Image of the lunar shadow cone over Europe taken by Meteosat-6 satellite (11th August, 1999, 10:50 UT). © 2001 EUMETSAT, http://www.eumetsat.de/en/area5/special/eclipse_11081999.html

However, the changes most available for observations concern local, micrometeorological parameters. The most important indicator of thermodynamical processes is air temperature in the boundary layer, which can be very easily measured.

It is reasonable to introduce a simple theoretical model of boundary layer thermal response in microscale. Including air temperature in low boundary layer.

The boundary layer air temperature depends in general on the flux of solar radiation and on some features of the ground (albedo, absorptivity, emissivity) and the features of the air (mainly

humidity). It can be claimed that these are mainly the conditions of heat transfer between the ground and the near-ground air layers that influence the air temperature most. The direct absorption of the solar shortwave radiation by air is negligible. The solar radiation is partially reflected by ground (or water) and partially absorbed. The ground irradiates a part of the energy by emitting thermal IR radiation (most intensive at ~15 µm), so in the range of larger wavelengths than the solar radiation (the corresponding value ~0,5 µm). This radiation is much better absorbed by the air in troposphere as it contains water vapour. The vital role in energy transfer between the ground and the air over its surface has, however, the processes of convection, which intensity depend on the vertical temperature gradient.

In order to model boundary layer air temperature changes, ground temperature variability during the eclipse should be known. The extraterrestrial radiation flux is essential factor shaping the ground parameters and it is necessary to predict its changes before. The model presented does not include any spectral changes.

The incident flux of direct solar radiation I can be expressed by Bouguer law:

$$I = I_0 \cdot p^m \cdot cos\ z \quad (3.1),$$

where I_0 means the instantaneous solar constant for the specified site, which decreases during the eclipse:

$$I_0 = S_0 \cdot (1 - g) \quad (3.2),$$

where $S_0 = 1372\ \text{W/m}^2$- solar constant, z - zenital angle of the center of solar disk, whose changes are known from ephemerides. p is transmission coefficient which depends both on the origin of the mass of the air over the considered area at specified time and on the local factors (pollutants emission) and is difficult to be predicted accurately, but its typical values vary from 0,7 to 0,9.

Integral air mass m may be given by frequently used Kasten and Young formula (Kasten, Young, 1989):

$$m = \left[cos\ z + 0.50572 \cdot (96.07995 - z)^{-1.6364} \right]^{-1} \quad (3.3).$$

Total net radiation can be given by the formula:

$$I = I_0 \left(0.36 + 0.74 \cdot p^{\frac{1}{cos\ z}} \right) \cdot cos\ z \quad (3.4),\ (\text{Blackadar, 1998}).$$

On the basis of ephemerides calculated in paragraph 2, a model of direct, scattered and total (net) radiation presented below was made (Fig. 4). It is compared with the values for the same day but with eclipse occurrence omitted.
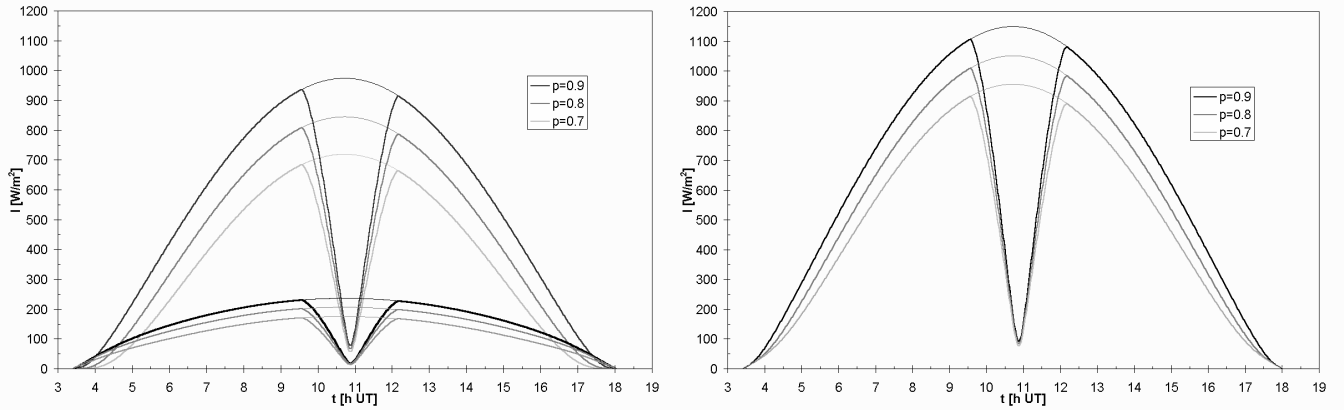
Fig.4. Modelled solar direct, scattered (left) and total (right) radiation flux in Szczawnica at the day of eclipse.

The further model is based on the assumption that system containing ground and boundary layer consists of homogenous horizontal layers (each layer has the same temperature in the whole volume). What is more, the temperature of the upper layer depends only on the temperature of the underlying layer and does not depend on the temperature of the upper layer.
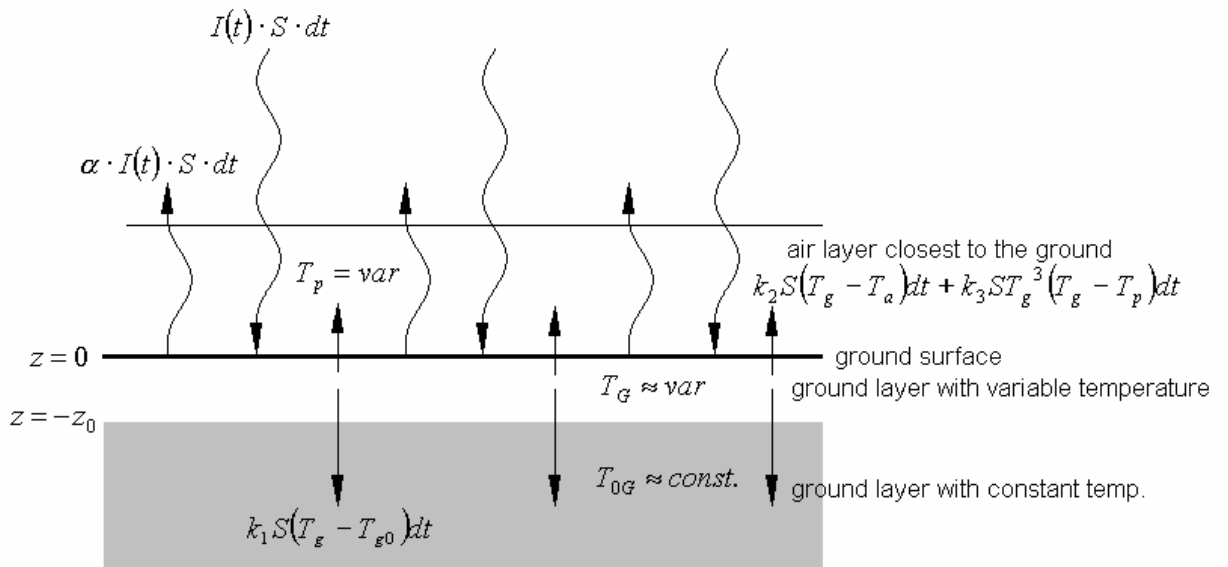

Fig. 5. Ground-air interaction model for predicting temperature changes due to eclipse.

Let the flux of radiation $I(t)$ fall on the theoretically separated surface of dry ground S characterised by integral albedo α (All further considerations assume dry air and ground). As even

annular temperature variability in the ground is limited to less than 1 m deep layer, we may assume that the changes take place only in the layer with $-z_0 \le z \le 0$ (z_0 is the length of temperature variations vanishing), so the ground is separated into two layers – superficial with temperature $T_g = T(-z_0 \le z \le 0)$ and the underlying layer with constant temperature T_{0g}. In both layers no temperature gradient exists ($\frac{\partial T_g}{\partial x} = \frac{\partial T_g}{\partial y} = 0$ and, according to the mentioned simplification,

$\frac{\partial T_g}{\partial z} \approx 0$). Then, according to the energy conservation law, we can write:

$$(1 - \alpha) \cdot I(t) \cdot S \cdot dt = c_m \cdot \rho \cdot z_0 \cdot S \cdot dT_g + k_1 S(T_g - T_{g0})dt + k_2 S(T_g - T_a)dt + k_3 S T_g^{\,3}(T_g - T_p)dt$$

(3.5),

where c_m - specific heat of the ground in superficial layer, ρ - its density, T_p - air temperature in the layer closest to the ground. The following terms on the right side describe: the changes of the ground temperature, the heat conduction to the deep layers of the ground, the heat transfer to the air by conduction on the ground surface, the heat transmission caused by the thermal radiation. All considered temperature differences are small (the differences do not exceed several per cent in the thermodynamic scale of temperature). We may omit any terms describing energy transfer between ground and air as the main process shaping the ground temperature is conduction to deep layers. This allows us to write:

$$a_1 \cdot A(t)dt = a_2 T_g dt + a_3 dT_g \quad (3.6).$$

This differential equation can be solved numerically, assuming the radiation flux time-dependent values are known from earlier considerations (given by the function (3.4)). In such situation T_g depends only on time and its initial value. Then it is easy to notify that:

$$\frac{dT_g}{dt} = b_1 A(t) - b_2 T_g \quad (3.7).$$

what can be substituted in Euler method by:

$$\left[\frac{\Delta T_g}{\Delta t}\right]_i = b_1 A_i(t) - b_2 T_{g_i}, \qquad T_{g_{i+1}} = T_{g_i} + \left[\frac{\Delta T_g}{\Delta t}\right]_i \Delta t \quad (3.8)$$

in the i-th iterative step, where Δt -the assumed time step.

The method described above allows to obtain the qualitative description of the progress of the ground temperature changes during the eclipse. The simulation starts at the sunrise and the initial superficial ground temperature refers to this time moment. It does not include many factors like ground parameters changeability with temperature, height, humidity and solar radiation spectral distribution, also neglects the temperature dependence of heat exchange factors.

As the difference in temperatures between air and ground is small, the term describing radiative energy transfer may have linear form by assuming $T_g^{\,3} \approx const.$. If the power of the ground-air heat transfer is proportional to the temperature difference and the air is submitted to isobaric processes, then the energy balance of the separated volume of air with temperature T_p, mass m and molar mass μ has the form of:

$$K\left(T_g - T_p\right)dt = \frac{m}{\mu}c_p dT_p \quad (3.9).$$

The equation omits the air radiation. It can be solved similarly to the previous one:

$$\frac{dT_p}{dt} = c_1\left(T_g - T_p\right) \quad (3.10).$$

In this case the ground temperature values are time-only-dependent variable known from the solution of (3.6).

In the sample model of air temperature changes in low boundary layer, the following coefficients were assumed:

$$\Delta t = 1, \;\; T_g\left(t = 3h25m\right) = 5, \;\; T_p\left(t = 3h25m\right) = 10, \;\; b_1 = 0.0005, \;\; b_2 = 0.008, \;\; d_1 = 0.05$$

The simulation for the day of eclipse starts at sunrise and ends at sunset. It has only qualitative features.
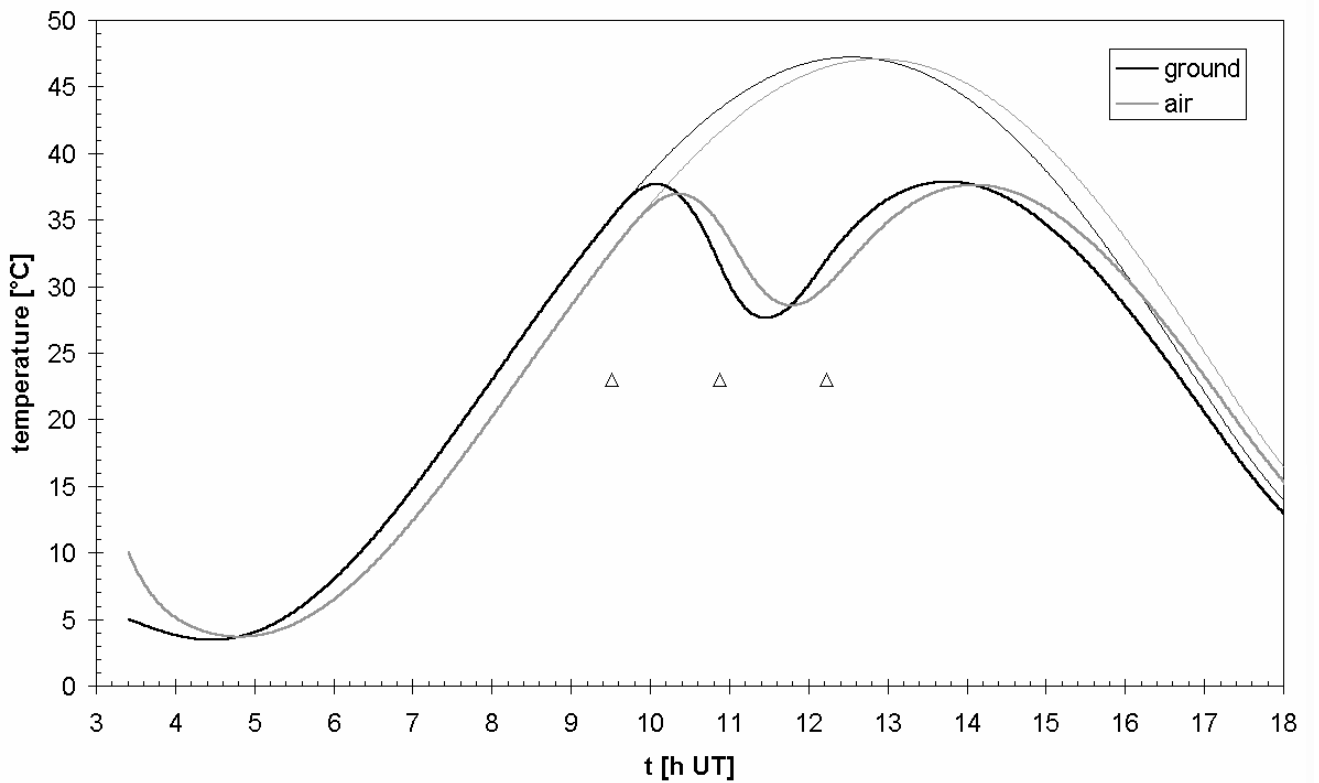

Fig. 6. Qualitative model of air and ground temperature changes during the eclipse in Szczawnica.

The chart (Fig. 6) presents the effect of numeric simulation of $T_g(t)$ and $T_p(t)$ functions for the mentioned model. The beginning, maximum and end of the eclipse were marked with triangles.

The model shows the characteristic time shift (delay) between the maximum obscuration of the eclipse and the moment of extremal value of temperature fall. It also depicts that the air temperature change has lower magnitude than ground temperature decrease. It illustrates the general influence on the daily temperature, which is significantly lower that modelled without eclipse. The time range with inversion occurs near the maximum of eclipse.

The model, as simplified one, does not show nocturnal temperature effects properly, but in this application it is not important.

4. Meteorological observations of the phenomenon.

4.1 The method

The phenomenon was observed from the terrace oriented southwards, placed on the last floor of the multistoreyed building.

The observations concerned the near-ground air temperature changes as well as the photometric studies of the brightness of the total sky and of the Sun-centred area. The self-constructed electronic 2-channel thermometer was used. The functioning of it is based on measuring the temperatures of two temperature sensors having different absorptivity, what allows for elimination of the influence of the solar radiation on the measured value. The thermometer contains two precise monolithic temperature-to-voltage converters LM35Z (TO-92 plastic case) (*National Semiconductor*), supplied with stabilised voltage. Both elements were placed on the horizontal cardboard stands, about 7.5 cm long, 6 cm wide, circa 3 cm over the artificial ground (black painted wooden surface) to assure air flow and prevent direct heat transfer from it. The upper surfaces were covered by aluminium foil to reduce intensive heating by the solar IR radiation. One of the sensors was tightly wound with a single piece of thin aluminium foil, the colour of the second one did not need a change as the package was black. The voltage between the output and circuit bulk is proportional to the temperature of the semiconductor junction expressed in degrees Centigrade with the factor of $k_T=10.0\ mV/°C$. The typical error of non-linearity does not exceed 0.2°C, the total temperature error is lower than 0.6°C. The values were not read exactly at the same time, but the time of switching did not exceed 3 seconds.

The time of reaching 90% of final voltage value after temperature change is ~2 minutes in still air. Taking it into account, the time interval between the measurements during the eclipse was matched to be 2 min. (1 min. close to the maximum).

Due to this feature of the device, low-pass filtering is assured and only long-period (several minutes) temperature fluctuations are remained.

For two sensors 1 and 2, characterised by different absorptivities, with identical heat capacities and in identical heat exchange conditions, the temperature difference between sensor and air is proportional to the incident radiation flux A (in terms of instantaneous thermal equilibrium):

$$\alpha_i A = a \cdot (T_i - T) \quad (4.1.1).$$

The absorptivity $\alpha_1 \approx 0.1$ for the aluminium foil, $\alpha_2 \approx 0.9$ for the black plastic case of the sensor (especially in IR range).

The real air near-ground temperature can be calculated from:

$$T = \frac{1}{k_T} \cdot \frac{\alpha_1 U_2 - \alpha_2 U_1}{\alpha_2 - \alpha_1} \quad (4.1.2).$$

The uncertainty of this value (the possible vertical shift of the curve) practically equals the maximal uncertainty in knowledge of temperature difference between the sensors, it means about 0.6°C. However the accuracy referred to the air temperature difference values is mainly limited by sensor non-linearity and does not exceed 0.2°C.

The auxiliary role was played by the determinations of the cloud cover taking place at the time of solar eclipse. Two-channel photometer, consisting of two photoresistors of type RPP 131 was employed. .

The first element was placed horizontally on the black, mat carton stand in the site illuminated directly by the Sun, close to the thermometer sensors. The field of view was only limited by the building's wall (opposite the position of the Sun) and the ceiling (over the estimated elevation ~70°). The second one was inside the mat tube with its field of view about 5° in diameter. The device was installed on the camera's case, leveled at the position of the solar disk and following the celestial sphere daily rotation with camcorder.

The resistances of both sensors were measured in 2-minute intervals. The measurements were based on determining the difference in resistance between both devices. Due to changes in cloud cover, the angular distribution of sky brightness was varying. In clear-sky conditions most of the radiation comes from the surrounding of the solar disk, so the light fluxes registered by both sensors should not differ. Contrary to it, when homogenous cloud cover exists, the sky brightness is almost constant over the whole range of angular distances from solar disk, so the light flux received by the sensor depends on its fields of view and the resistance of the whole-sky sensor is expected to be lower. The sensor's resistance depends on the illumination E in the range of resistances measured during the eclipse according to:

$$E \sim R_f^{-(1.10 \pm 0.02)} \quad (4.1.3).$$

The functioning of the device is independent on the total radiation intensity (it is, however, sensitive to sky brightness angular distribution changes). During the solar eclipses the ratio of zenith illuminance to horizontal illuminance remains does not change towards its normal, clear-sky value (Darula at al., 2001). The measurements let know the time moments when the important cloud cover appeared and the solar disk was covered. They were compared with the visual estimations of the level of solar disk coverage by clouds, as it was registered by camcorder and good correlation between these methods was found.

4.2. The results and discussion
4.2.1 The cloud cover

The results of the cloud cover measurements (relative difference in illuminances referred to total illuminance) are presented on the chart (Fig. 7).
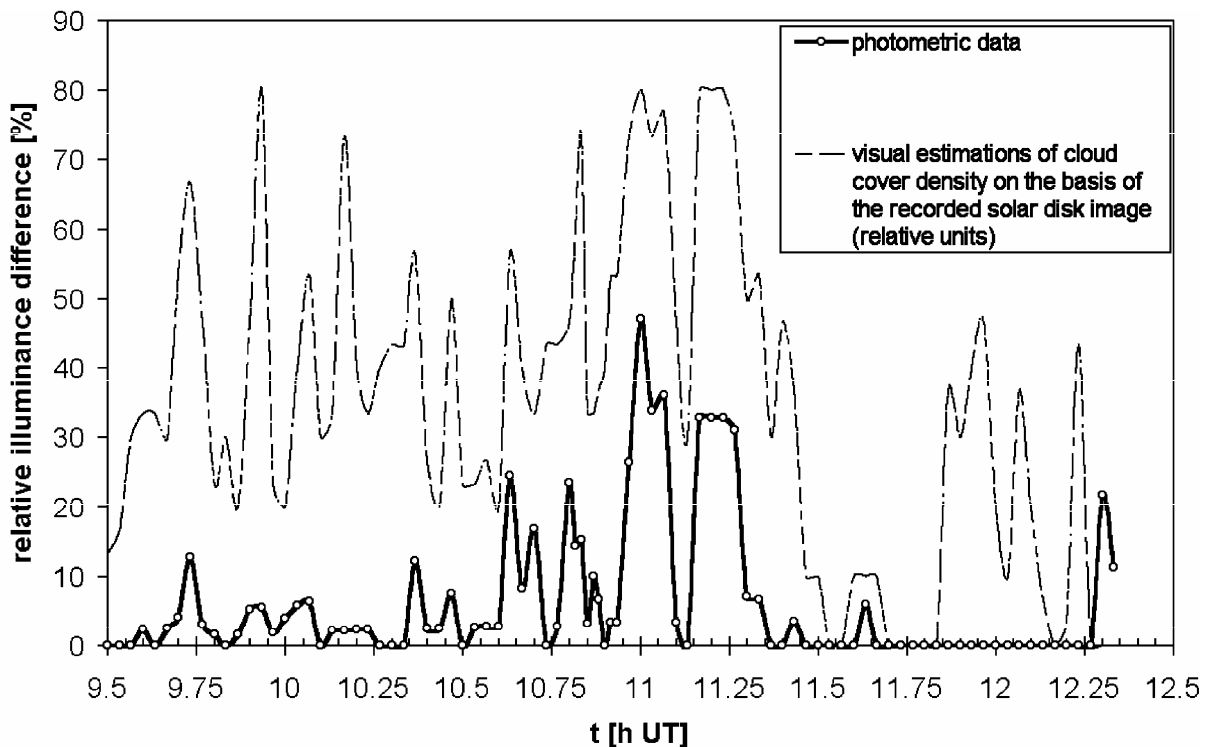

Fig. 7. Relative difference in both sensors' illumination, being the measure of the cloud cover.

It must be noticed that the most dense cloud cover corresponds with the maximum eclipse. The zero values do not indicate clear sky. As it was obtained from recorded film, cloud cover was not present only near the middle of the second part of phenomenon, and the during rest of the time of observation thin clouds were present. The variability of cloud cover is large (observations were made in 2 min. intervals). This is not advantageous, but similar conditions influenced the conditions of observation in the whole Central Europe (fig. 8).
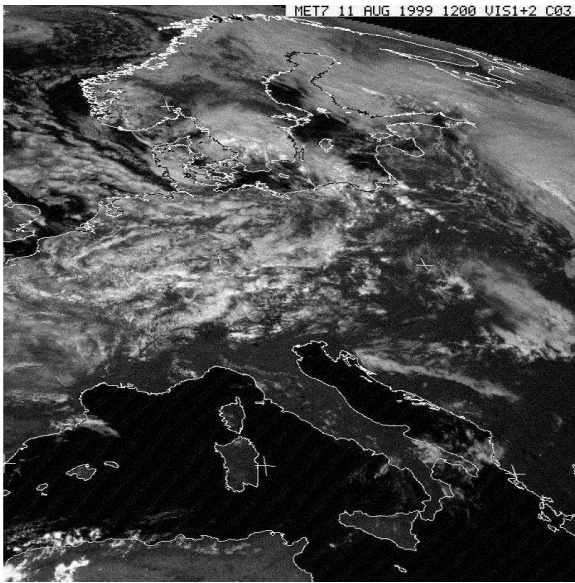
Fig. 8. Overview of general meteorological situation over Central Europe after the maximum of the eclipse (the images near to the maximum are almost dark). Thanks to the courtesy of the University of Nottingham,
http://www.nottingham.ac.uk/meteosat/eclps99/

It is sometimes stated that the mechanism responsible for the cloud cover appearing near the time of the maximal eclipse exists. Their formation is presumed to be caused by water vapour condensation due to temperature decrease. This mechanism requires specific conditions, regarding the fact that the temperature decrease on high altitudes does not have large magnitude. It is not possible to separate this hypothetical effect from the general cloud cover variability over the specified site of observation.

4.2.2 The air temperature curve general features

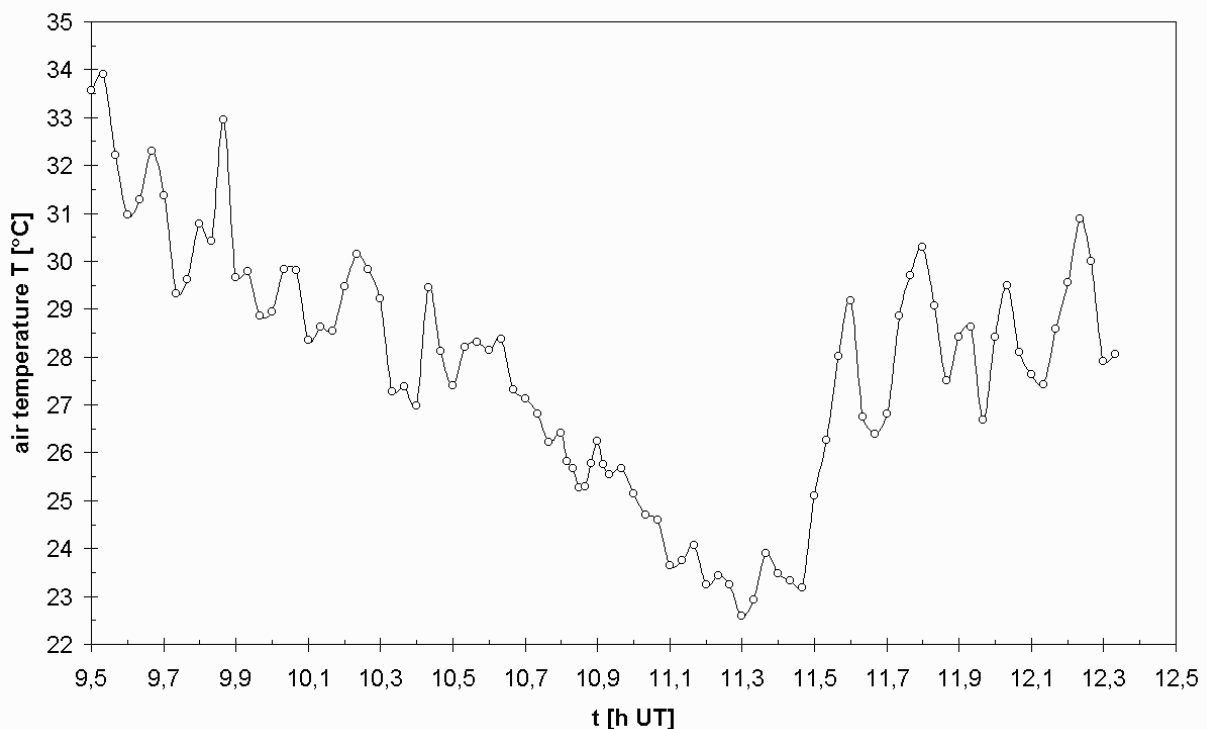The registered near-ground air temperature changes curve is shown on the chart (Fig. 9).

Fig. 9. Near-ground temperature changes during the eclipse.

If comparison with usual meteorological data is needed, it is important to notice that the temperature was measured 3 cm over the artificial ground, while typical meteorological measurements are done on the height of 2 m.

It is interesting to notify that the temperature decrease began in fact at the moment of the 1st contact. Due to ground-air system properties, the presence of a delay is expected. The air temperature minimum, however, showed the characteristic delay towards the moment of maximal obscuration g. The maximal temperature decrease value was circa 11°C, about 11:18 – 25 min. after the maximum (its value for air temperature it depends on the type of climate and increases with height over the ground). It can be compared with the value of 20 min. registered by Foken et al. for total eclipse and temperature measured 6 m above the ground). The decrease value was considerably great, but it has to be emphasised that the temperature was measured very close to the ground having high absorptivity.

4.2.3. The influence on convectional events.

It is clearly noticeable from the visual inspection of the fig. 8. that two time ranges with different magnitude of temperature fluctuations exist on the graph, what is depicted by measure points spread. This spread corresponds to long-period fluctuational component T' of the temperature $T(t) = \overline{T}(t) + T'(t)$. The time range between 10:30 and 11:18 is characterised by considerable decrease of fluctuations intensity. It is commonly assumed that a temperature variance $\sigma_{T'}$ is a good measure of convectional turbulent fluctuations intensity (Lumley, Panofsky, 1966). The analysis of the variance is direct when the mean temperature $\overline{T}(t)$ varies negligibly (as it happens especially for short measurement series for investigating high frequency temperature fluctuations in stable weather conditions). On the opposite, such measurements of long-period fluctuations are more difficult, because even relatively slow-acting non-convectional factors may overlap the temperature changeability over a period of a few hours which is necessary. The special difficulty is caused by eclipse-connected rapid change of mean temperature. So when calculating the variance $\sigma_{T'}$, the shape of $\overline{T}(t)$ function must be known. The fluctuation process is random what implicates $\overline{T'} = 0$ and allows for $\overline{T}(t)$ estimation by least-squares fit. Then $\overline{T}(t_i) = T_{pred}$ and the residuals $T_{obs}(t_i) - T_{pred}(t_i) = T'(t_i)$ for each realisation of temperature measurement in time instant t_i. The usage of running mean was also taken into consideration, but obtained result was not smooth enough and indicated some oscillations (which could be removed only by averaging wider range of

measurements). The mentioned oscillations could produce misleading results of spectrum analysis in the range of long periods. In our opinion, it is very advantageous to employ smooth function (polynomial of the low degree). Moreover, it is not necessary to find one function for total time range, but different function for each range can be applied. This is possible as the total range will be divided into separate subranges with visually different temperature variance. The ranges (assumed arbitrary) are in table 2.

Table 2. Time ranges for temperature analysis.

A	B	C	D
9:30 – 10:34	10:34 – 11:22	11:22 – 11:36	11:36 – 12:20

For this reason thwe function can be non-smooth in the points limiting the ranges. In final data handling, linear functions were used for ranges B, C and D and parabolic function was fitted to A range points. The effects of such fitting and the residuals are plotted in figs. 10 a,b.
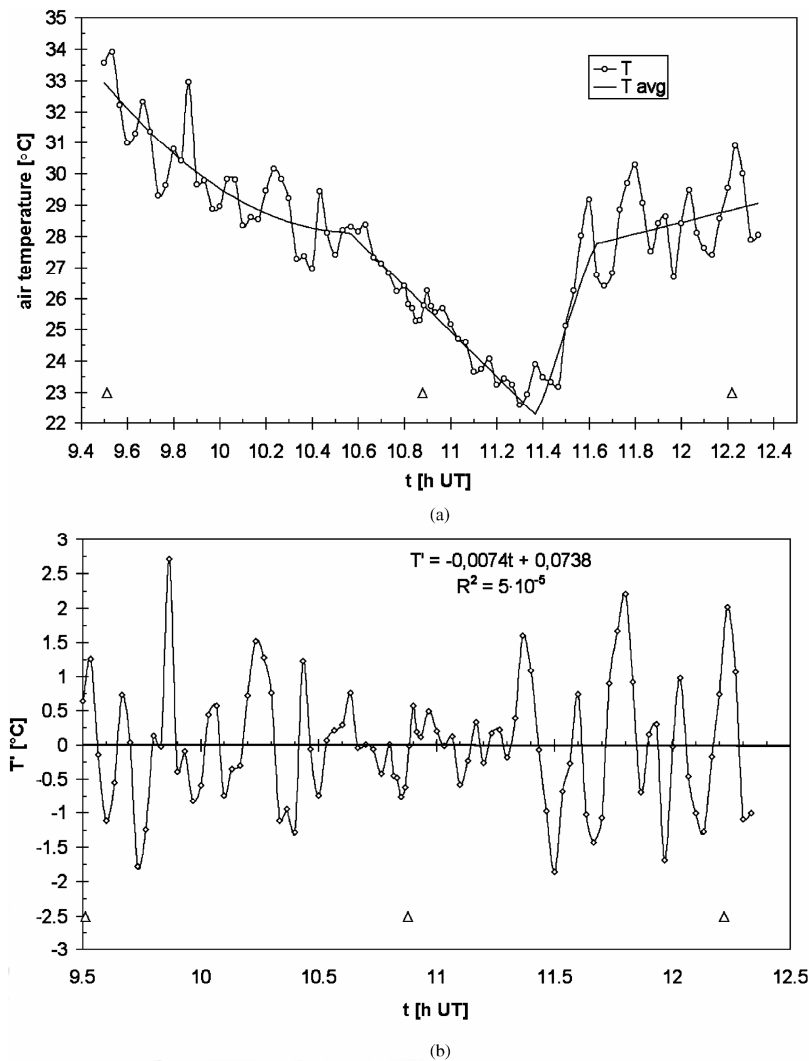

(a)

(b)

Fig. 10. (a) The measured temperature towards the fitted model of mean temperature.

(b) Residual values for air temperature.

The measure of quality of smoothing is that the regression line fitted to residuals (showed on the plot) which is almost exactly equal to zero.
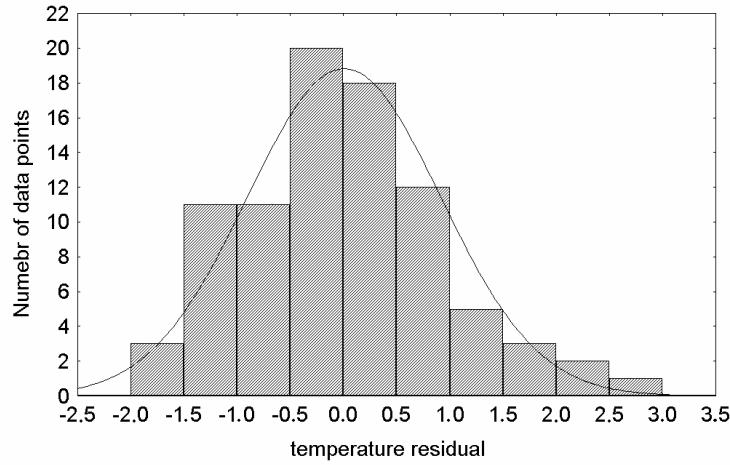

Fig. 11. The histogram of the residuals over the whole series of measurements. Normal distribution curve fitted.

The temperature variance for each range is presented in table 3.

Table 3. Variance and its uncertainty (normal distribution assumed) for temperature analysis ranges.

Time range	A	B	C	D
$\sigma_{T'} \pm \sigma_{\sigma_{T'}} \ [^{\circ}C]$	0.98±0.13	0.38±0.05	1.15±0.29	1.17±0.18

As the variance value depicts convection intensity, it is obvious that B range is characterised by its noticeable decrease. The range of much reduced convection covers approximately 25 minutes before and after maximum. It is in excellent consistence with data obtained by Foken et al., 2001, showing 1 hour long, totality-centred time range with low fluctuations magnitude. On the basis of the theoretical model, we should observe that before maximum eclipse thermal inversion takes place what produces stable stratification, which is expected to vanish with restoration of normal stratification, after the maximum.

The FFT was applied to such prepared residuals. However, this method has disadvantage, namely it may indicate poor resolution for short time intervals and the results may show the leaking effect. The suitability of such methods to convection investigations is discussed by Petenko and Bezverkhnii, 1999. The discrete wavelet transform (DWT) is advised, but this algorithm has even worse resolution. DWT is advantageous when longer data series are considered. The undoubted positive feature of wavelet transform is the ability of presenting the changes of power distribution vs time. In our opinion FFT is better method for this data handling, as time dependence of spectra

is obtained by analysing separate data ranges and better resolution is required. In order to increase the resolution, the common method of padding the time series with zeroes was used (50 zeroes were concatenated to each range residuals sample). This leads to more smooth spectral density function. Windowing was used additionally with Hamming weighs and averaging of 5 periodogram points. The effects are depicted on the two plots in linear and logarithmic scale. (fig. 12). The range C was not analysed as too short.
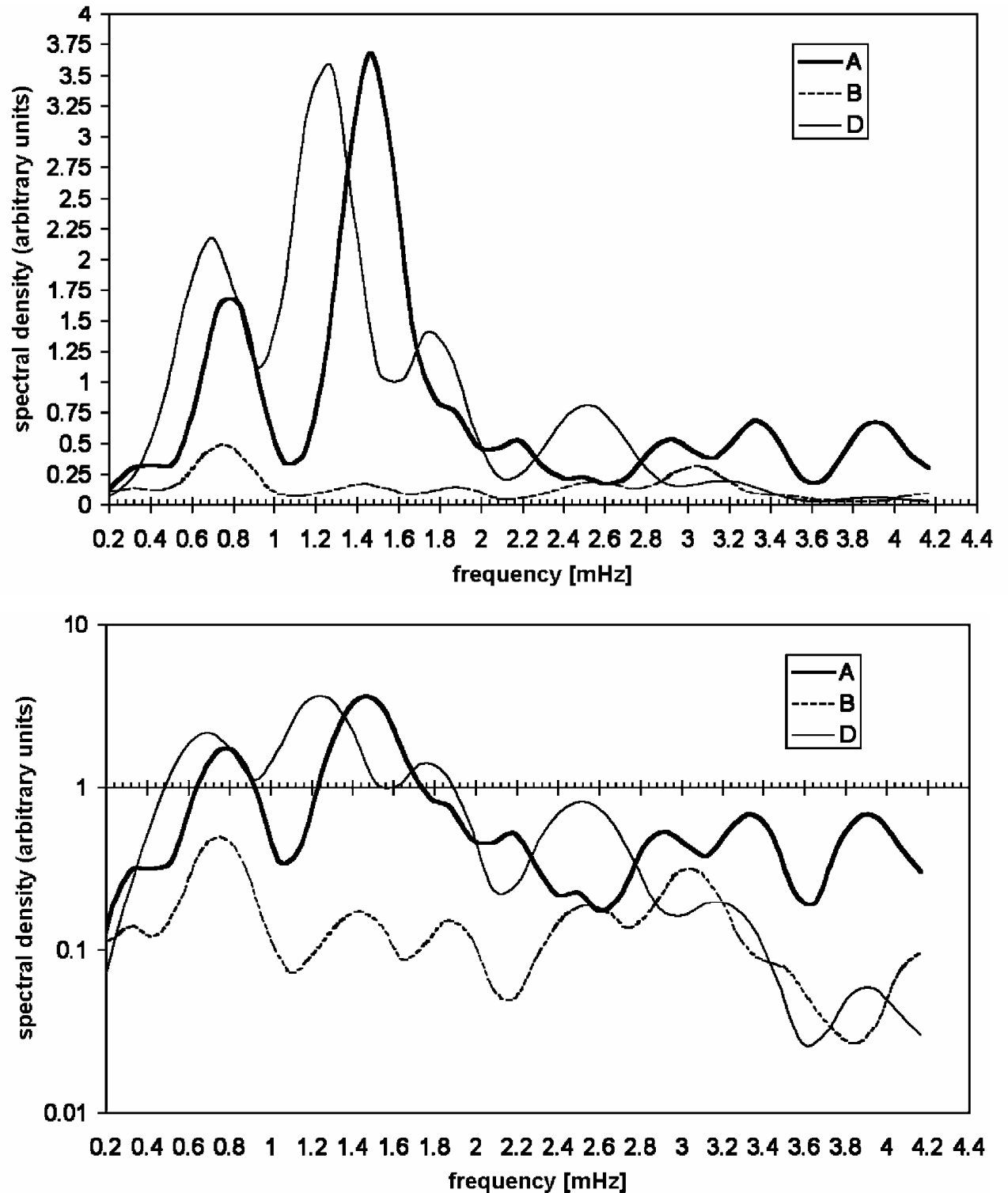
Fig. 12. FFT spectra of thermal fluctuations for ranges A, B and D.

The graphs show that the spectra for the ranges A and D are very similar and both indicate strong, two-peak maxima at 11-13 and 22-24 minutes. This is generally consistent with the temporal convective scales obtained by Petenko and Bezverkhnii, 1999. They conclude the presence of significant temporal scales of 7-9 and 18-22 minutes, but, under the conditions of less-developed convection, the 11-16 min. scale replaces the longer one. According to their data, the temporal scale increases with convection development. The behaviour of smaller scales is explained by the structure of large convectional plumes that consist of smaller ones. The spectrum for B series (covering the time near of maximal obscuration) is significantly different. The lower peak of the two-peak maximum (22 min.) increases while the second one (11-13 min.) is much reduced. What is more, an additional maximum with shorter period of 5.5 min. occurs. The most noticeable effect is the decrease of the fluctuations intensity by a factor of 10. The temporal scales during 1999 eclipse were investigated by Foken et al., 2001. As it was mentioned, their results indicate convection intensity reduction around totality, and the total absence of fluctuations with period shorter than 3 minutes. They also conclude that shorter time scales occur in coincidence with cloud cover appearance (see especially their figure 3b, page 177).

Our conclusion concerning temporal scale is that the development of longer timescale (22 min) is due to eclipse and the shorter one (5.5 min) might be caused by cloud cover. It also might be stated that the smaller convectional plumes become more "sharp" as the convection intensity decreases. It should be connected with the character of the structure of large plumes that consist of smaller ones. We must emphasise that cloud cover intensity increased much during the maximum and before and it overlapped the eclipse effect. However, it is not possible to separate both factors. For more accurate conclusions, further investigations using continuous wavelet transform are desired (they show temporal changes of fluctuations intensity in different time scales in continuous manner).

5. Conclusions.

The observations confirmed that the occurrence of the stable stratification in the low boundary layer can be expected due to solar eclipse phenomenon occurrence. The general fall of convection intensity is visible in temperature fluctuation component variance decrease at least by a factor of 2. The temporal scales of convection analysed on the basis of temperature fluctuating component variance FFT obtained inside 1 hour maximum eclipse-centred time range seem to be different from ones observed under the typical conditions. It was not possible to separate effects of eclipse and of changeable cloud cover, but the increase of the temporal scale seem to take place. The most important temporal scale changes form 11-13 min. to 22 min. The behaviour of such parameters can

only be explained by analysis of the convectional plums structure and interactions between larger plumes that consist of smaller ones.

Only if microscale processes are known in details, it is possible to simulate the mesoscale effects of eclipses.

6. Acknowledgements

7. References

Bamford, R.A., 2001. The effect of the 1999 total solar eclipse on the ionosphere. Physics and Chemistry of the Earth, Part C: Solar, Terrestrial & Planetary Science **26C** (5), 373-377.

Blackadar, A.K., 1997. Turbulence and Diffusion in the Atmosphere. Lectures in Environmental Sciences. Springer-Verlag Berlin, Heidelberg, New York.

Boška, J., Šauli, P., 2001. Observations of gravity waves of meteorological origin in the F-Region ionosphere. Physics and Chemistry of the Earth, Part C: Solar, Terrestrial & Planetary Science, **26C** (6), 425-428.

Chudzyński, S., Czyżewski, A., Ernst, K., Pietruczuk, A., Skubiszak, W., Stacewicz, T., Stelmaszczyk, K., Szymański, A., Sówka, I., Zwoździak, A., Zwoździak, J., 2001. Observation of ozone concentration during the solar eclipse. Atmospheric Research, **57** (1), 43-49

Darula, S., Kambezidis, H. D., Kittler, R., 2001. Daylight levels during the solar eclipse of 11 August 1999. Meteorology and Atmospheric Physics **76** (3/4), 251-256.

Espenak, F., Anderson, J., 1997. Total Solar Eclipse of 1999 August 11, NASA RP 1398, Greenbelt.

Fabian, P., Rappenglück, B., Stohl, A., Werner, H., Winterhalter, M., Schlager, M., Stock, P., Berresheim H., Kaminski, U., Koepke, P., Reuder, J., Birmili, W., 2001. Boundary layer photochemistry during a total solar eclipse. Meteorologische Zeitschrift **10** (3), 187-192.

Foken, T., Wichura, B., Klemm, O., Gerhau, J., Winterhalter, M., Weidinger, T., 2001. Micrometeorological measurements during the total solar eclipse of August 11, 1999. Meteorologische Zeitschrift **10** (3), 171-178.

Kasten, F., Young A. T., 1989. Revised optical air mass tables and approximation formula. Applied Optics **28** (22), 4735-4738.

Koepke, P., Reuder, J., Schween, J., 2001. Spectral variation of the solar radiation during an eclipse. Meteorologische Zeitschrift **10** (3), 179-186.

Petenko, I.V., Bezverkhnii, V. A., 1999. Temporal scales of Convective Coherent Structures Derived from Sodar Data. Meteorology and Atmospheric Physics **71** (1/2), 105-116.